공학석사 학위논문

Analysis of orientation of the transition dipole moment of phosphorescent dyes in the energy-transferring condition

에너지 전달 조건에서 인광염료의 쌍극자 모멘트 방향 분석

2014년 2월

서울대학교 대학원

재료공학부

문 창 기

Analysis of orientation of the transition dipole moment of phosphorescent dyes in the energy-transferring condition

지도 교수 김 장 주

이 논문을 공학석사 학위논문으로 제출함

2014 년 2 월

서울대학교 대학원

재료공학부

문 창 기

문 창 기 의 석사 학위논문을 인준함

2014 년 2 월

위 원 장 윤 재 륜 (인)

부위원장 김 장 주 (인)

위 원 서 용 석 (인)

Abstract

Analysis of orientation of the transition dipole moment of phosphorescent dyes in the energy-transferring condition

Chang-Ki Moon

Department of Materials Science and Engineering

The Graduate School

Seoul National University

The dipole orientation of an emitter is one of the key factors influencing the out-coupling efficiency in OLEDs. Polymers or small molecules with linear or disk shape have been known to have preferred orientation. On the other hand, globular shape phosphorescent molecules, especially iridium complexes are believed to be randomly oriented. However, recently some phosphorescent molecules are reported to have preferred orientation along the horizontal direction parallel to the substrate when deposited by thermal evaporation.

However, factors influencing the orientation of the transition dipole moment of the Ir based phosphorescent dyes in thin films have not been studied yet. This thesis reports that types of main ligand and ancillary ligand of Ir complexes could lead to have preferred dipole orientation. Moreover, effects of the doping concentration and the excitation condition were studied as factors influencing the orientation.

Keywords: organic light emitting diodes, phosphorescent dyes, dipole orientation, angle-dependent photoluminescence, optical simulation, energy transfer

Student Number: 2012-20598

Contents

List of Tables

List of Figures

Chapter 1. Introduction

1.1 Organic Light-Emitting Diodes

Organic light emitting diodes (OLEDs) are successfully in use not only as small size displays and but also as large size TVs and solid state lighting. OLEDs extend their application to flexible displays and transparent displays which are not easily achievable with liquid crystal displays. White OELDs have also been developed for displays and solid state lighting and their efficiency reaches the efficiency of fluorescent lamp with better color rendering index and warm color. Moreover, there are large rooms for further improvement of efficiency in OLEDs to be a future high quality lighting source combined with low energy consumption. Figure 1.1 illustrates some examples of OLEDs in the lighting and displays. These achievements are good examples to show the potential and future prospect of OLEDs.

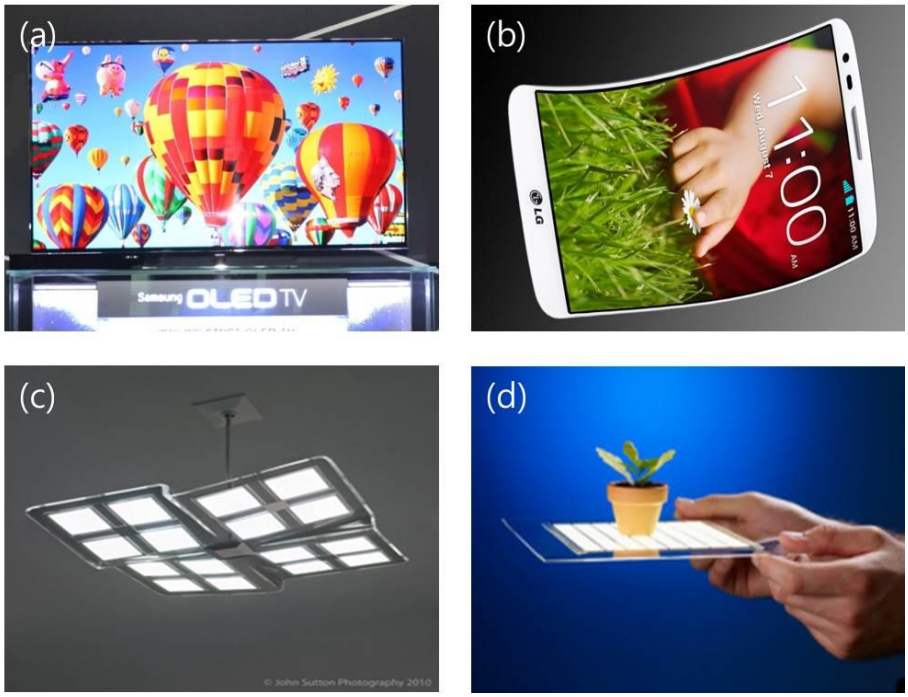

Figure 1.1 Examples of the application of OLEDs (a) OLED TV (Samsung, 2012). (b) Curved OLED display mobile phone (LG, 2013). (c) OLED lightings (LG, 2010) (d) OLED lightings (Novaled, 2010).

1.2 The basic structure and operation of OLEDs

The basic structure of bottom emission OLEDs is illustrated in figure 1.2, which is composed of substrate / transparent anode / hole transporting layer (HTL) / emitting layer (EML) / electron transporting layer (ETL) / metal cathode. Single or double organic layer OLEDs are also possible but other layers can contribute to enhance charge carrier injection and transportation properties. Electrons injected from the cathode and holes from the anode recombine in the emitting layer to form excitons. Because of the Fermionic nature of electrons, singlet and triplet excitons are formed with the ratio of 1:3 if the excitons are formed statistically. Fluorescent molecules can harvest the singlet energy to light and the triplet energy is lost to heat. In contrast, phosphorescent molecules can convert both singlet and triplet energy to light so that theoretically 4 times higher efficiency can be achieved using phosphorescent dyes than fluorescent dyes. The emitted light in the OLEDs must be outcoupled to air through a transparent electrode. Because of the high refractive indices of the organic layers, transparent electrode and substrate, only 20~30% of the emitted light can be outcoupled if the transition dipoles are randomly oriented and rest of the emitted light is confined in the device.

The ratio of the outcoupled photons to the injected electrons is called the external quantum efficiency (EQE), i.e.,

$$\eta_{EQE} = \frac{the\ number\ of\ emitted\ photons\ to\ outside}{the\ number\ of\ injected\ charge\ carriers} \quad (1.1)$$

Based on the light emitting process describe above, the EQE can be expressed as follows as

$$\eta_{EQE} = \gamma \cdot \eta_{S/T} \cdot q \cdot \eta_{out} \quad (1.2)$$

where γ is the charge carrier balance factor, $\eta_{S/T}$ is the factor representing the ability to convert the singlet and triplet excitons to photon energies ($\eta_{S/T}$ is 0.25 for fluorescent molecules and 1 for phosphorescent molecules), q is the radiative quantum efficiency of excitons, and η_{out} is the outcoupling efficiency. Up to recent years, photoluminescent (PL) quantum yield of a material measured in solution or in thin films were used as q and the outcoupling efficiency was considered as independent from the quantum efficiency. However, q itself is influence by the location in a cavity structure such as OLEDs and the out coupling efficiency depends on the location of the emitter in the OLEDs, which will be described in the next section. [1-3]

Since the first three terms in the right side of equation (1-2) are related to the light emission process inside OLEDs, the above equation is sometimes expressed in a simplified form as

$$\eta_{EQE} = \eta_{IQE} \cdot \eta_{out} \quad (1.3)$$

where η_{IQE} is the internal quantum efficiency.

The internal quantum efficiency can be raised up to near 100% with advances of molecules and device structures. However, the outcoupling efficiency is not much high because photons are generated in an environment of high refractive index (n ~ 1.7) and they should escape out to the air (n = 1). It was expected about 17~20% if calculated by simple ray optics. However, OLEDs having EQEs over 30% have been reported recently, [1] which could not be explained by the ray optics. The appropriate theoretical limit of EQE and other optical properties of OLEDs can be well described by the classical dipole model with the electromagnetic wave theory.

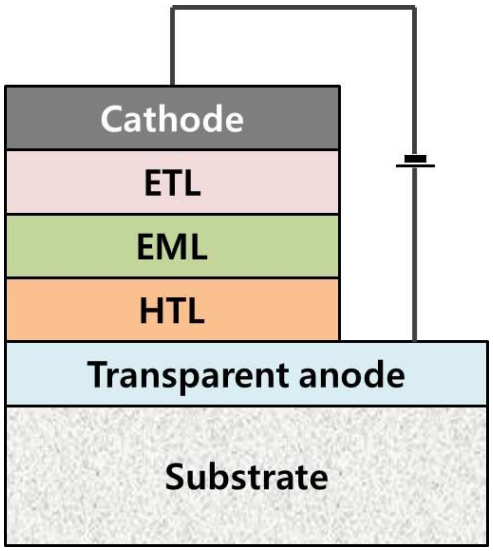

Figure 1.2 Schematic description of OLED structure

1.3.2 Optical modeling – the dipole model

The optical simulation of OLEDs used in this thesis is based on the classical dipole model. The OLEDs are composed of a stack of very thin layers comparable to wavelength of visible light. Moreover, the radiative decay rate of emitting molecules in thin film doesn't agree with that in free space, which is called Purcell effect. [4] Therefore, the light generated in the OLEDs should be treated with the electromagnetic wave theory. The dipole model which described molecular fluorescence and energy transfer of an emitting dipole near planar interfaces was suggested by Chance, Prock, and Silbey (CPS). [5] This model was developed and modified to apply to OLEDs by many researchers. [3, 6-8]

The dipole near interfaces was regarded as a forced damped harmonic oscillator. The equation of the motion of the dipole was expressed as

$$m\frac{d^2x}{dt^2} + mb_0\frac{dx}{dt} + m\omega_0^2 x = eE_R \qquad (1.3)$$

where m is the effective mass of the dipole, x is the displacement of the dipole, b_0 is the decay rate in free space, ω_0 is the resonant angular frequency, e is the electric charge constant, and E_R is the reflected electric field. Otherwise, it can be expressed with dipole moment ($\mu = mx$)

$$m\frac{d^2\mu}{dt^2} + b_0\frac{d\mu}{dt} + \omega_0^2\mu = \frac{e^2}{m}E_R\,. \tag{1.4}$$

The dipole and the reflected electric field oscillate with the same complex frequency $\Omega = (\omega_0 + \Delta\omega) - i(b/2)$, where b is the decay rate near interfaces. Then, solutions of μ and E_R are expressed as

$$\mu = \mu_0 exp(-i\Omega t)\,, \tag{1.5}$$

$$E_R = E_{R,0} exp(-i\Omega t)\,. \tag{1.6}$$

Substituting μ and E_R, the equation (1.4) is

$$(-\Omega^2 - i\Omega b_0 + \omega_0^2)\mu_0 = \frac{e^2}{m}E_{R,0}\,, \tag{1.7}$$

and the solution is

$$\begin{aligned}\Omega &= -i\frac{b_0}{2} + \omega_0\sqrt{1 - \frac{b_0^2}{4\omega_0^2} - \frac{e^2}{m\mu_0\omega_0^2}E_{R,0}} \\ &\approx -i\frac{b_0}{2} + \omega_0\left(1 - \frac{b_0^2}{8\omega_0^2} - \frac{e^2}{2m\mu_0\omega_0^2}E_{R,0}\right)\end{aligned} \tag{1.8}$$

with assumptions that $b_0^2 \ll \omega_0^2$ and $\frac{e^2}{m\mu_0}E_{R,0} \ll \omega_0^2$. Dividing Ω into real and imaginary parts, the b and the $\Delta\omega$ are

$$b = b_0 + \frac{e^2}{m\mu_0\omega_0^2}Im(E_{R,0})\,, \tag{1.9}$$

$$\Delta\omega = \frac{b_0^2}{8\omega_0^2} + \frac{e^2}{2m\mu_0\omega_0^2}Re(E_{R,0})\,. \tag{1.10}$$

The clssical formula for the radiatve decay rate is [9]

$$b_r = \frac{2e^2 k_1^3}{m\omega n_1^2} \tag{1.11}$$

where n_1 is the refractive index of the medium containing the dipole and k_1 is the wave vector in the medium. Because the radiative quantum efficiency is $q = b_r/b$, equation (1.9) can be rewritten with the normalized decay rate ($\hat{b}$) as

$$\hat{b} = \frac{b}{b_0} = 1 + \frac{e^2}{b_0 m\mu_0\omega_0^2} Im(E_{R,0}) = 1 + \frac{3qn_1^2}{2\mu_0 k_1^3} Im(E_{R,0})\,. \tag{1.12}$$

Now, the decay rate is modified by the reflected electric field. The solution of the electric field radiated from a dipole near interfaces was investigated early by Sommerfeld [10] who used a Hertz vector potential (Π) in cylindrical coordinates. This method gave the solution of decay rate of each dipole aligned vertically and horizontally to the interface. When the emitting layer is sandwiched by two layers like an OLEDs environment as illustrated in figure 1.3, the normalized decay rates of vertically ($\perp$) and horizontally ($\parallel$) aligned dipoles are given as follows:

$$\hat{b}_{\perp,\parallel} = \frac{b_{\perp,\parallel}}{b_0} = 1 - qZ_{\perp,\parallel}\,, \tag{1.13}$$

$$Z_\perp = 1 - \frac{3}{2} Im \int_0^\infty \frac{F\left(\hat{d}, -R_{12}^{\parallel}\right) F\left(\hat{s}, -R_{13}^{\parallel}\right)}{F\left(\hat{d}+\hat{s}, -R_{12}^{\parallel} R_{13}^{\parallel}\right)} u^3 \frac{du}{l_1}, \tag{1.14}$$

$$Z_{\parallel} = 1 - \frac{3}{4} Im \int_0^{\infty} du \frac{u}{l_1} \left[\frac{F\left(\hat{d}, -R_{12}^{\perp}\right) F(\hat{s}, R_{13}^{\perp})}{F\left(\hat{d} + \hat{s}, -R_{12}^{\perp} R_{13}^{\perp}\right)} + (1 - u^2) \frac{F\left(\hat{d}, R_{12}^{\parallel}\right) F\left(\hat{s}, R_{13}^{\parallel}\right)}{F\left(\hat{d} + \hat{s}, -R_{12}^{\parallel} R_{13}^{\parallel}\right)} \right] \tag{1.15}$$

where u is the normalized in-plane wave vector, $l_n = -\mathrm{i}(\varepsilon_n/\varepsilon_1 - u^2)^{1/2}$, ε_n is the dielectric constant in n th medium, $F(x, y) = 1 + yexp(-2l_1 x)$, $\hat{d} = k_1 d$, $\hat{s} = k_1 s$, and $R_{nm}^{\perp,\parallel}$ is the Fresnel's reflection coefficient of perpendicular and parallel dipoles from medium n to m. The transfer matrix method can be used to calculate the reflection coefficient of a multi-layer structure [11]. When the dipole distribution of the emitter is isotropic, the normalized decay rate is a combination of that of perpendicular and parallel dipoles, which is expressed as

$$\hat{b}_{iso} = \frac{1}{3} \hat{b}_{\perp} + \frac{2}{3} \hat{b}_{\parallel} . \tag{1.14}$$

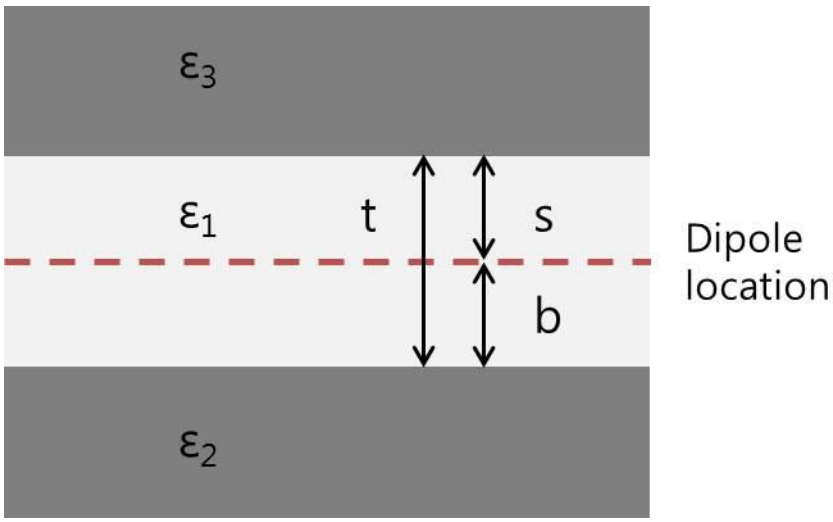

Figure 1.3 An environment of dipoles at emitting layer sandwiched by two layers.

The normalized decay rate also can be decribed with the relative power dissipation function (P).

$$\hat{b} = 1 - q + q \int_0^\infty P du. \tag{1.15}$$

Therefore, the quantum efficiency of emitter in OLEDs is now modified as

$$q_{eff} = \frac{\hat{b}_r}{\hat{b}} = \frac{q \int_0^\infty P du}{1 - q + q \int_0^\infty P du}. \tag{1.16}$$

The integration of the power disspation function corresponds to Purcell factor in the cavity.

The light generated in OLEDs couples to different optical modes. Since organic layers in OLEDs are very thin and have higher refractive index than air, much amount of light was confinend inside as waveguide modes. Some of the light is reflected back at the glass/air interface, some is absorbed to metal electrodes and other escape out to air. These optical modes can be distinguish ed by propating direction of light or, more precisely, in-plane wave vector (u) in the power dissipation function.

Their optical modes are devided by the k_{air}, $k_{substrate}$, and k_{orgnic} which are products of wavevector in free space ($\lambda/2\pi$) and refractive indices of their media. If the in-plane wave vector is $0 < u < k_{air}$, the light can radiated to air (out-coupled). In the same manner, if the in-plane wave vector is $k_{air} < u < k_{substrate}$, their power is confined in the substrate (substrate mode). If the in-plane wave vector is $k_{substrate} < u < k_{orgnic}$, their power

is confined in the organic layer (waveguided mode). If the in-plane wave vector is $k_{orgnic} < u < \infty$, they absorbed to electrodes as suface plasmon polaritons (SPPs mode).

1.4 Effects of dipole orientation of phosphorescent dyes in OLEDs

To obtain highly efficient OLEDs, the internal quantum efficiency (η_{IQE}) and the out-coupling efficiency (η_{out}) which were stated in equation (1.2) should be increased. Quantum mechanics said that $\eta_{S/T}$ is 0.25 for fluorescent emitters but 1.0 for phosphorescent emitters in general. Therefore, phosphorescent dyes have been used to obtain high efficiency. [12-15] Phosphorescent dyes had been regarded as having isotropic dipole distribution due to their octahedral and globular molecular structures as shown in figure 1.4. However, some phosphorescent dyes have been reported to have preferred dipole orientation [14, 16-19] in organic host materials (table 1.1).

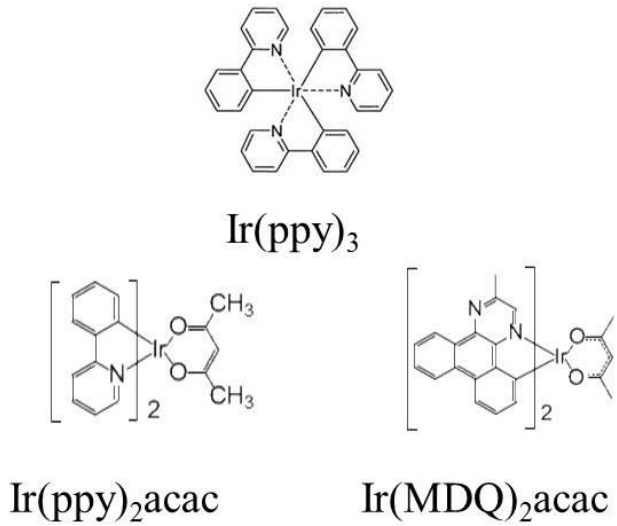

Figure 1.4 Molecular structures of some phosphorescent dyes.

Table 1.1 Summary of dipole orientation of phosphorescent dyes in the literature

Year	Publishing group	Dyes	Dipole orientation (hori. : verti.)
		Isotropic dye	67:33
2011	W. Brütting	$Ir(MDQ)_2acac$	Mainly horizontal
2011	N. Danz	$Ir(MDQ)_2acac$	76:24
2012	K. Neytz	$Ir(MDQ)_2acac$	80:20
2012	K. Leo	$Ir(ppy)_2acac$	77:23
2013	J.-J. Kim	$Ir(ppy)_2acac$	77:23

Orientation of transition dipole moment (dipole orientation) of an emitter plays important role in η_{out}. A dipole emits light propagating along the perpendicular direction to the dipole axis as illustrated in figure 1.5a. Figure 1.5b schematically shows the radiations from horizontally and vertically oriented dipoles in OLEDs. The light emitted from the horizontally aligned dipole largely propagates vertically against the substrate so that large transmittance is expected. In contrast, the light emitted from the vertical dipole propagates horizontally and most of the light is not outcoupled from OLEDs. The effect of dipole orientation can be obtained from the dipole model**.** The normalized decay rate in equation (1.14) can be rewritten with the proportion of the horizontal dipole moment (α),

$$\hat{b} = (1-\alpha)\hat{b}_{\perp} + \alpha\hat{b}_{\parallel}\,. \qquad (1.17)$$

According to optical simulation, horizontally oriented dipoles give 1.5 times higher out-coupling efficiency than the isotropic distribution. [1] Therefore, determination of the dipole orientation now becomes an important work. This thesis reports the dipole orientation of phosphorescent dyes and factors influencing the orientation. The Chapter 2 describes a modified set up of angle dependent photoluminescence (PL) measurement with improved accuracy of the measurement of the orientation. The modified experimental set up was used to measure the orientation of several phosphorescent dyes which are described in Chapter 3. Doping concentration dependent dipole orientation was described in Chapter 4 followed by summary in Chapter 5.

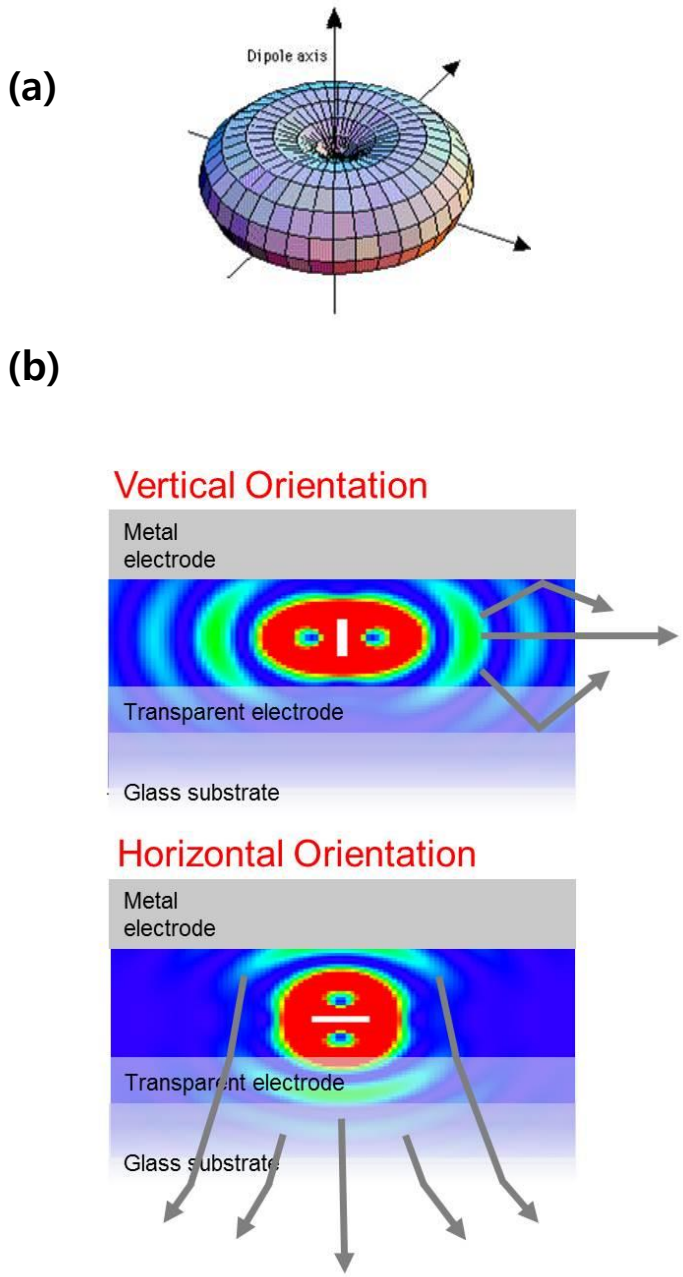

Figure 1.5 (a) The dipole radiation in free space. (b) The schematic diagrams of radiation from dipoles which aligned vertically and horizontally to the substrate of OLEDs.

Chapter 2. Modification of angle-dependent PL measurement set up for improved resolution

2.1 Experiments

2.1.1 Films fabrication

Organic film was deposited onto 1 mm thick fused silica substrate by thermal evaporation under 10^{-7} torr without breaking vacuum. The bis(2-phenylpyridine)(acetylacetonate)iridium(III) [$Ir(ppy)_2acac$] was co-evaporated with 4,4′-Bis(N-carbazolyl)-1,1′-biphenyl [CBP] to get the total thickness of 30 nm. Weight ratio of the film was controlled 8 wt% for $Ir(ppy)_2acac$ and 92wt% for CBP. The film was encapsulated to prevent degradation.

2.1.2 Angle-dependent PL measurement

Angle-dependent PL measurement was used to determine orientation of $Ir(ppy)_2acac$. The detection wavelength was 520 nm. The influence of CBP emission was neglected. Only p-polarized light was measured by using a polarizer. First, the conventional experimental method was used. Next, the improved method was used with the same film.

2.2 The improvement in angle-dependent PL measurement

The angle-dependent PL measurement [20] was used in this study to analyze the dipole orientation of phosphorescent dyes. This method determines the dipole orientation by fitting the angle-dependent PL intensity of a thin film using an optical simulation. It is useful to analyze the orientation of not only fluorescent film but other emitting materials by doping in a matrix whose optical constants are known. According to the literature, the error of dipole orientation determined by this method was ±4%. The conventional

experimental set up is described in figure 2.1. The film is excited by laser whose incident angle was 45° and emits photons to the substrate. They go out through the half-cylinder prism without reflection because both half cylinder prism and substrate are composed of fused silica. In general, only p-polarized light is obtained by a polarizer but s-polarized light is also possible. Figure 2.2 shows angular emission patterns of the CBP:Ir$(ppy)_2$acac 8wt% film measured by this method. However, this method had problems in data symmetry and reproducibility. There was a strange peak only on the positive angle. It gave poor reproducibility and large error ranges

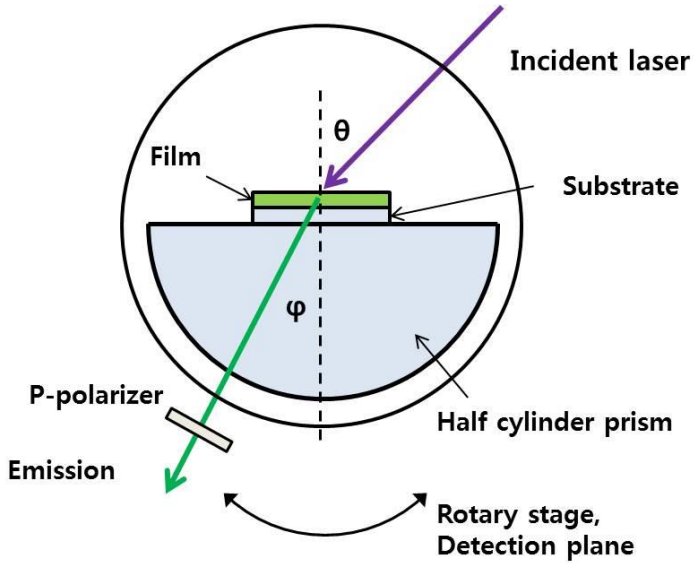

Figure 2.1. An experimental set-up of the angle-dependent PL measurement. The incident angle of laser is 45°

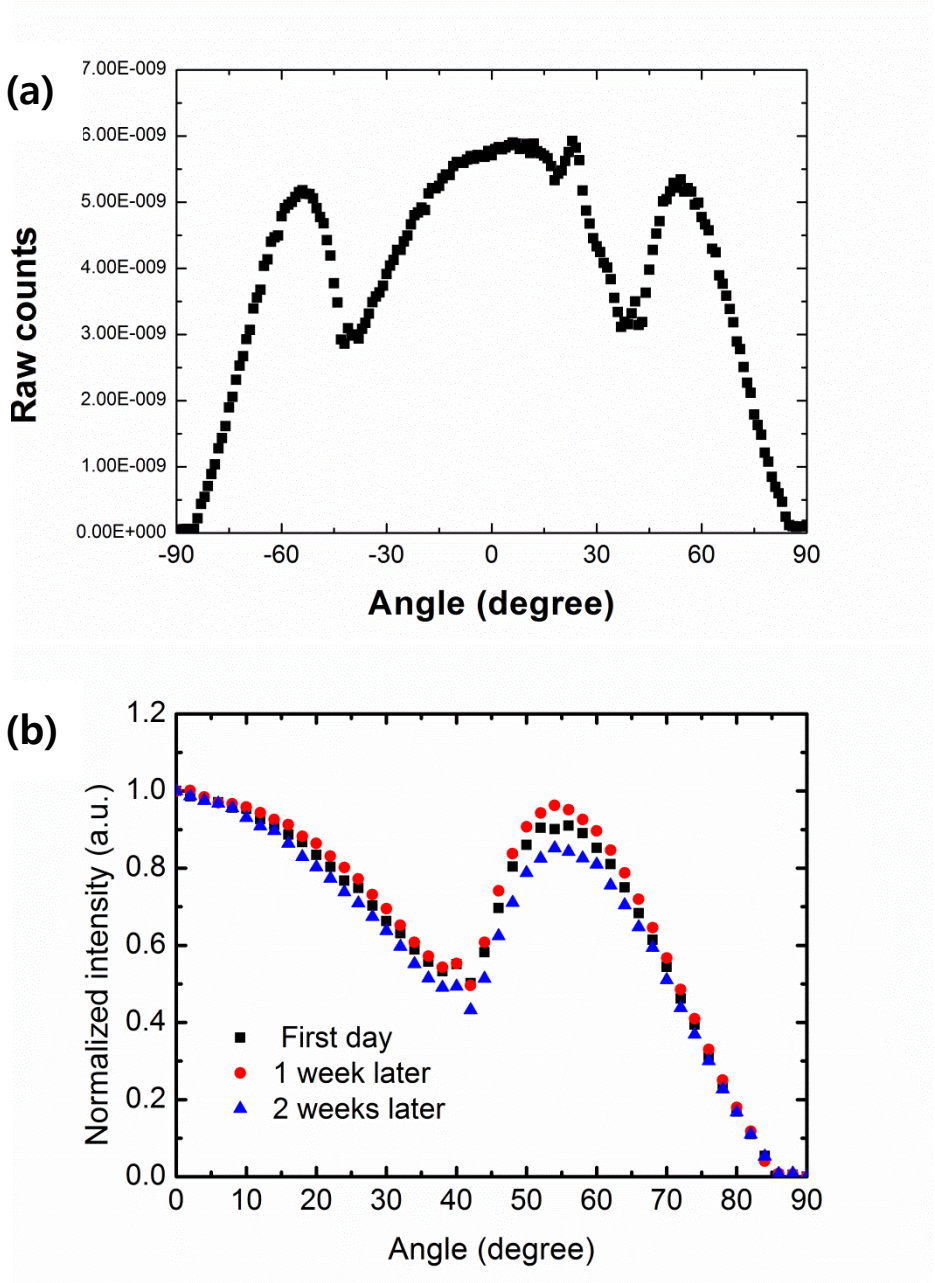

Figure 2.2 Results of angle-dependent PL. The results showed (a) a strange peak near +24° and (b) poor reproducibility

By calculation of Fresnel's refraction law, it was verified that the strange peak near +24° was on the way of the laser incidence. Therefore, the direction of incidence was adjusted to be set out of the detection plane. Figure 2.3 schematically illustrates refinement in the laser incidence. The angle of incidence was 45° to excite all dipoles equally. As a result, influences of incident light were eliminated. Symmetrical results could be obtained with good reproducibility. The measurement error was enhanced to ±1%. Figure 2.4 shows improvements in symmetrical data and good reproducibility in measurement.

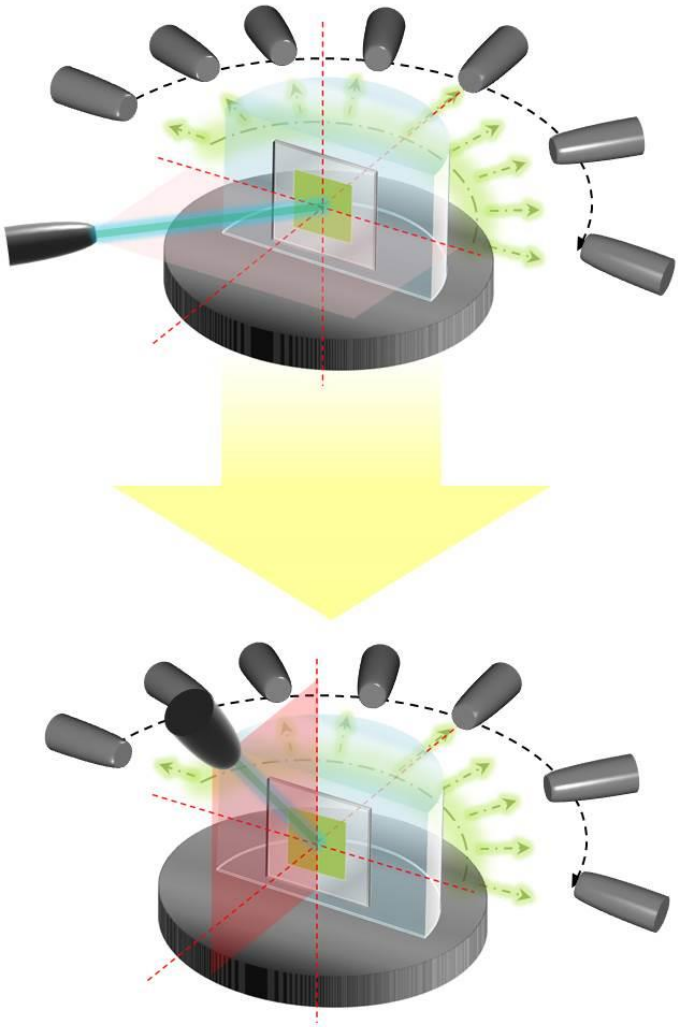

Figure 2.3 Refinement in measurement. The direction of incidence was adjusted to be out of detection plane

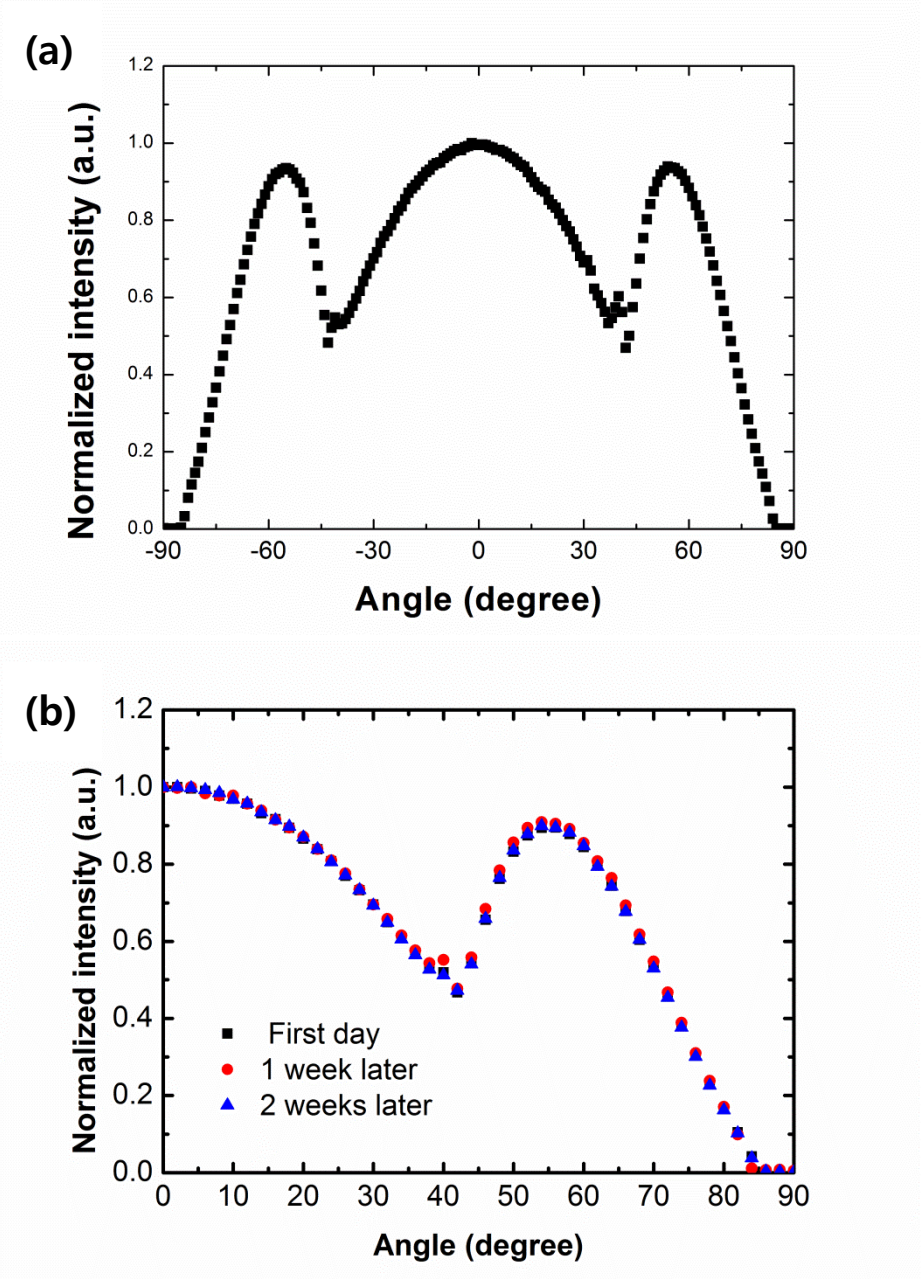

Figure 2.4 Results of angle-dependent PL by the refined method. There were improvements in (a) data symmetry and (b) reproducibility

Chapter 3. Dipole orientation of phosphorescent dyes

3.1 Experiments

3.1.1 Films fabrication

Organic films were deposited onto 1 mm thick fused silica substrate by thermal evaporation under 10^{-7} torr without breaking vacuum. 6 different phosphorescent dyes of tris((3,5-difluoro-4-cyanophenyl)pyridine) iridium [FCNIr], bis[2-(4,6-difluorophenyl)pyridinato-C2,N](picolinato)iridium(III) [FIrpic], tris[2-phenylpyridinato-C2,N]iridium(III) [$Ir(ppy)_3$], bis(2-phenylpyridine)(acetylacetonate)iridium(III) [$Ir(ppy)_2acac$], tris[1-phenylisoquinoline-C2,N]iridium(III) [$Ir(piq)_3$], and bis(2-methyldibenzo[f,h]quinoxaline)(acetylacetonate)iridium (III) [Ir(MDQ)2acac] were separately co-evaporated with CBP to get the total thickness of 30 nm. Doping concentration of all dyes were 8 wt%.

3.1.2 Angle-dependent PL measurement

The modified experimental set up in chapter 2 was used to measure the dipole orientation of phosphorescent dyes. The detection wavelength was 470 nm, 520 nm, and 610 nm. The influence of CBP emission was neglected. Only p-polarized light was measured by using a polarizer.

3.2 Emission patterns of 6 phosphorescent dyes

Dipole orientation of 6 kinds of blue – [FCNIr, FIrpic], green – [$Ir(ppy)_3$, $Ir(ppy)_2acac$], and red – [$Ir(piq)_3$, $Ir(MDQ)_2acac$] phosphorescent dyes was determined. Dyes were doped in the CBP matrix which could give their energy to dyes. Refractive index of the CBP which was necessary for optical simulation was measured by the variable angle spectroscopic ellipsometry (VASE). We took detection wavelength to 470 nm, 520 nm, and 610 nm for blue, green, and red dyes. Figure 3.1 shows the refractive index of the CBP and simulated angle-dependent emission patterns of 30nm CBP film at each wavelength in case of isotropic and 100% horizontally aligned dipole distribution. It was assumed films were excited uniformly in simulation.

Angular emission patterns of each dye were plotted in figure 3.2 as violet scatters. It was investigated that each dye has its own emission pattern. It said that dyes have their own dipole orientation in spite of their globular structures.

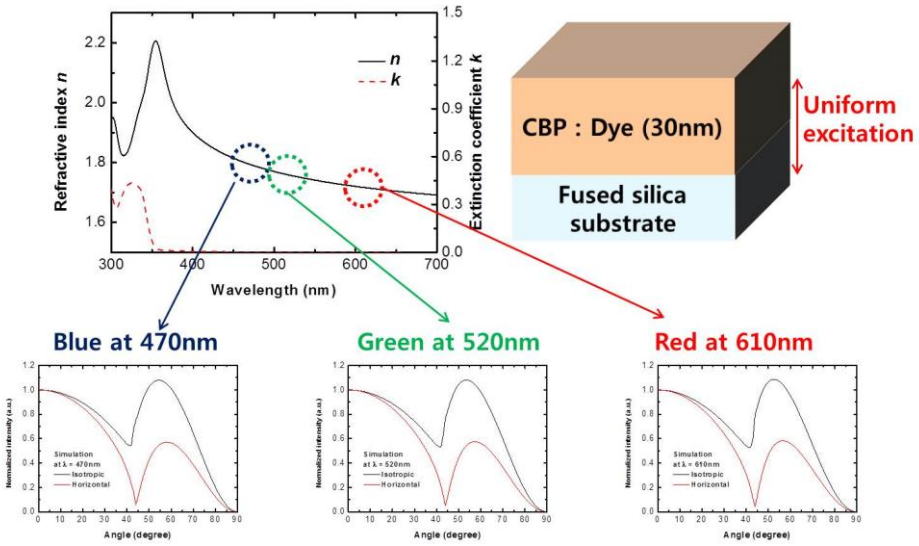

Figure 3.1 The refractive index of CBP and simulated angular emission patterns of dipoles in the 30nm CBP film. Emissions for isotropic and 100% horizontally aligned dipole distribution were calculated at each wavelength of blue, green, and red.

3.3 Dipole orientation of 6 phosphorescent dyes

Their orientation was determined by fitting with optical simulation which followed the equation:

$$I_p(\theta) = \alpha\, I_{p,h}(\theta) + (1-\alpha) I_{p,v}(\theta) \qquad (2.1)$$

where α is the proportion of the horizontally aligned dipole, I_p is intensity of p-polarized light and h, v indicate horizontal and vertical dipole. The factor α is 2/3 for isotropic orientation and could be varied for other specific orientation. As shown in figure 3.3 their emission patterns matched very well with the simulation. The dipole orientation of each phosphorescent dye was described in table 3.1. The $Ir(ppy)_3$ had nearly isotropic dipole orientation but other dyes had horizontally preferred dipole orientation. When the molecules were classified by having ancillary ligands or not, heteroleptic molecules had horizontal dipoles more than homoleptic molecules. They seem to have the preferred orientation by inter-molecular interaction with their asymmetric molecular structures. In spite of homoleptic structure, FCNIr and $Ir(piq)_3$ showed preferred orientation rather than isotropic distribution. They have electron withdrawing substituents or bulky benzene rings compared to $Ir(ppy)_3$. In these results, it should be possible to control the dipole orientation of Ir complexes by modifying molecular shapes and substituents.

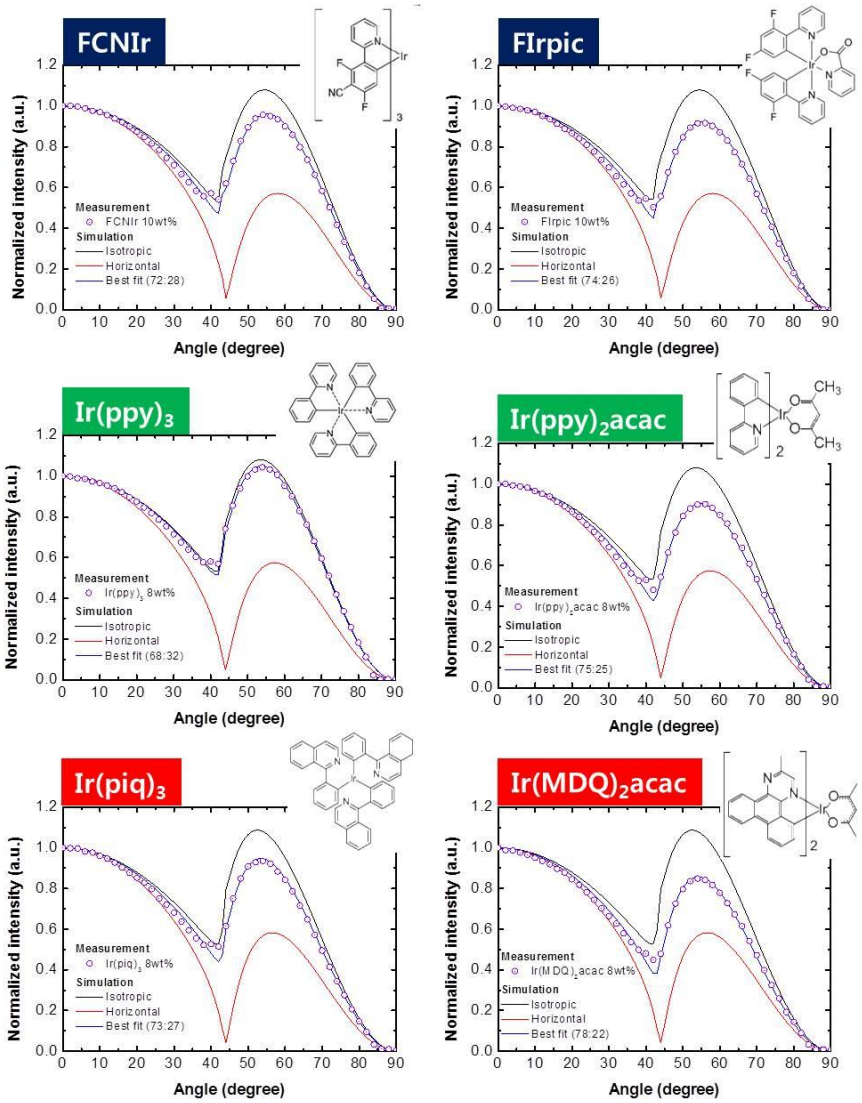

Figure 3.2 Angular emission patterns of 6 phosphorescent dyes and their fittings of the orientation.

Table 3.1 Summary of dipole distribution of 6 phosphorescent dyes.

Color	Dyes	Dipole distribution (horizontal : vertical)
Blue	FCNIr	72 : 28
	FIrpic	74 : 36
Green	$Ir(ppy)_3$	68 : 32
	$Ir(ppy)_2acac$	75 : 25
Red	$Ir(piq)_3$	73 :27
	$Ir(MDQ)_2acac$	78 : 22

Chapter 4. Doping concentration dependence of the dipole orientation in the energy transferring condition

4.1 Experiments

4.1.1 Films and OLEDs fabrication

Organic films and OLEDs were fabricated by thermal evaporation under 10^{-7} torr without breaking vacuum. The films were deposited onto 1 mm thick fused silica substrate and the OLEDs were deposited onto 0.7 mm thick glass substrate which was pre-coated with 70 nm ITO. The films were composed of bis(2-phenylpyridine)(acetylacetonate)iridium(III) [$Ir(ppy)_2acac$] doped in 4,4′-Bis(N-carbazolyl)-1,1′-biphenyl [CBP) with different concentrations. The thickness of the film was fixed to 30 nm. The concentrations of $Ir(ppy)_2acac$ were 0, 0.1, 0.2, 0.5, 1, 2, 4, 8, and 16 weight percent (wt %). The OLEDs were designed to have simple structures using 2,2′,2″-(1,3,5-benzinetriyl)-tris(1-phenyl-1-H-benzimidazole (TPBi) as a ETL for simplicity in optical

simulation. The OLEDs were fabricated following these sequences: glass / ITO (70nm) / MoO_3 (1 nm) / CBP (45 nm) / CBP with $Ir(ppy)_2acac$ doping (30nm) / TPBi (20nm) / $RbCO_3$ doped TPBi (125 nm). The concentrations of $Ir(ppy)_2acac$ were 1 and 8 wt%.

4.1.2 PL spectra measurement

PL spectra were measured by photomultiplier tube (PMT). Films were fixed onto a jig and the detector was located at the normal direction of films. Two kinds of lasers were used for excitation. One is a He-Cd laser (CW, 325 nm) and the other is a semiconductor diode laser (CW, 405 nm).

4.1.3 Angle-dependent PL measurement

Angle-dependent PL measurement was used to analyze orientation of $Ir(ppy)_2acac$. The detection wavelength was 520 nm and the influence of CBP emission was neglected.

4.1.4 Characterization of the OLEDs

The J-V-L characteristics were analyzed with the Keithley 2400 and the SpectraScan PR 650 (Photo Research). The angle-dependent EL spectra were measured by an Ocean Optics S2000 fiber optic spectrometer with constant current. OLEDs were fixed in programmed rotary stage during angular spectra measurement. The EQE was calculated by the ratio of between the numbers of emitted photons and injected electrons. The EQE was first calculated by the emission spectrum at normal direction with an assumption of the Lambertian distribution. Next, the EQE was calibrated with the angular emission distribution of actual devices.

4.2 Dipole orientation of $Ir(ppy)_2acac$ in films

4.2.1 PL spectra

PL spectra were measured with the 325 nm excitation. Results of PL spectra with different doping concentration from 0.1 wt% to 16 wt% is illustrated in figure 4.1. The PL intensity of CBP gradually reduced with increase of doping

concentration. The emission of CBP was suppressed at high doping concentration over 8wt%. Simultaneously, the PL intensity of $Ir(ppy)_2acac$ around 520 nm increased until 4 wt% but reduced as doping concentration increased. It indicated that CBP host molecules were excited first and gave their energy to $Ir(ppy)_2acac$.

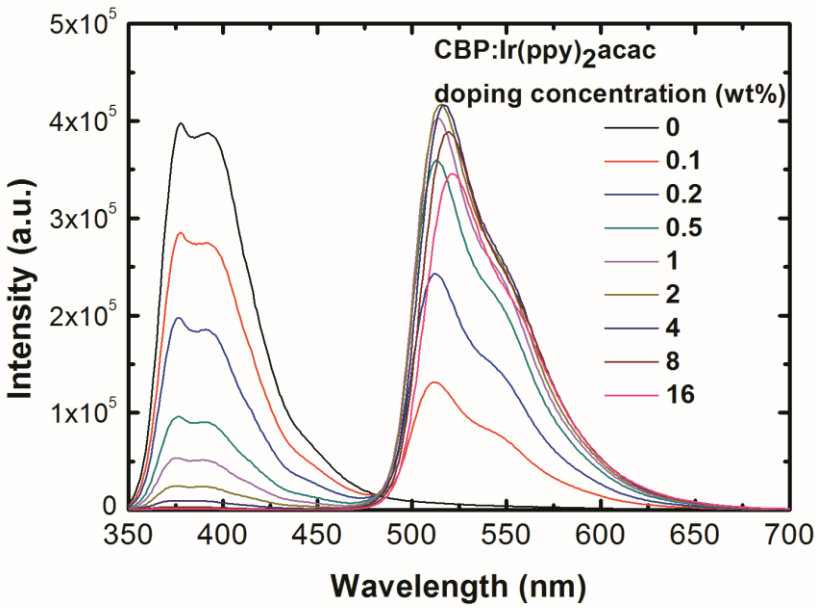

Figure 4.1 PL spectra of CBP:Ir(ppy)$_2$acac films depending on the doping concentration.

4.2.2 Angle-dependent PL patterns

Figure 4.3 shows results of angle-dependent PL of the films at 520 nm wavelength with the 325 nm excitation. All results were normalized to 0 degree. Angular emission patterns are plotted in figure 4.2. At high doping concentration of 8, 16 wt% they showed same emission patterns. However, as doping concentration decreased from 8 wt%, the relative intensity around 55° gradually went up. This result said that the dipole orientation of $Ir(ppy)_2acac$ gradually changed with the doping concentration until high concentration over 8 wt%.

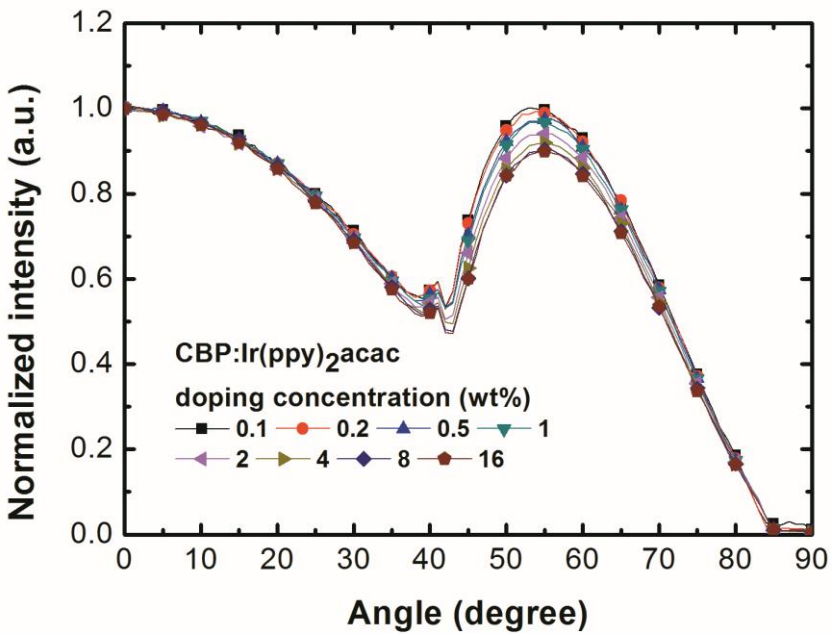

Figure 4.2 Angle-dependent PL of CBP:Ir(ppy)$_2$acac films depending on doping concentration. Relative intensity around 55° went up as doping concentration decreased from 8 wt%.

4.2.3 Fitting and determination of dipole orientation of $Ir(ppy)_2acac$

The dipole orientation of $Ir(ppy)_2acac$ was determined by fitting of the angle-dependent PL measurement with optical simulation. Figure 4.3a shows two examples of determining the orientation of 0.1 wt% and 8 wt% $Ir(ppy)_2acac$. These two films showed obviously different emission patterns. To find out specific orientation, the emission pattern from that film was calculated by optical simulation and they are plotted in figure 4.3a. Little difference of film thickness and refractive index was neglected in this optical simulation. Both measurements were located between simulated emission patterns of isotropic and perfectly horizontal dipole cases. The pattern of 1 wt% film was more close to isotropic orientation than that of 8 wt%. By adjusting proportion of the horizontal dipoles (α) in simulation which was expressed as equation (2.1), the most appropriate dipole orientation was determined. Measurements and fittings matched very well when the proportion of the horizontal dipole α = 0.70 for 0.1 wt% film and α = 0.75 for 8 wt% film. All dipole orientation of the films was analyzed in the same manner. As a result, the value of α decreased as doping concentration decreased. The α was 0.75 at high concentration but it gradually decreased to 0.70 at lower concentration than 8 wt%.

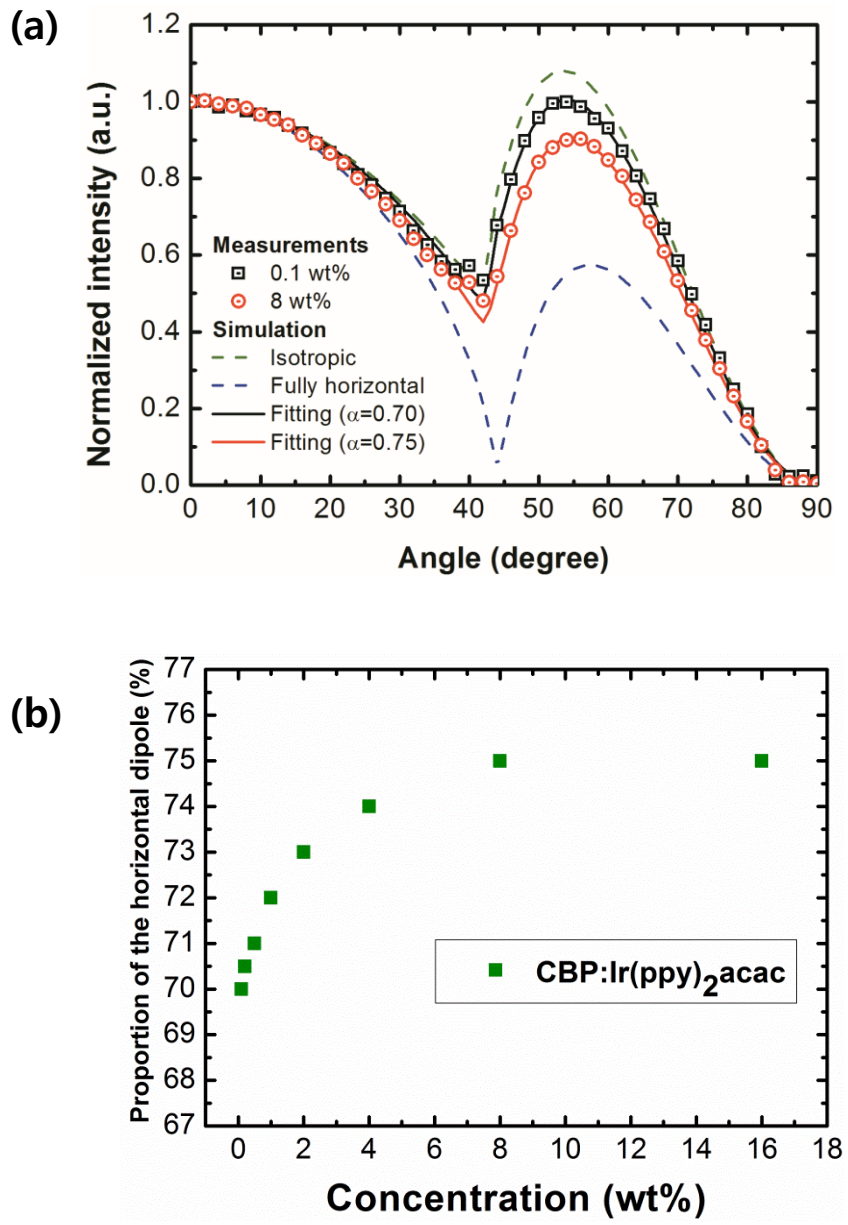

Figure 4.3 (a) Angle-dependent PL of the 0.1 wt% and 8 wt% films. They were fitted when α = 0.7 and 0.75. (b) All determined dipole orientation of $Ir(ppy)_2acac$ doped in films. The value of α decreased as doping concentration decreased.

4.3 Dipole orientation of $Ir(ppy)_2acac$ in OLEDs

4.3.1 Device structures

OLEDs were designed to observe the change of dipole orientation depending on the doping concentration with electric driving. The CBP and $Ir(ppy)_2acac$ composed the EML as the host and the dopant. Two kinds of OLEDs whose concentrations of the emitter were 1 wt% (OLED 1) and 8 wt% (OLED 2) were fabricated. The structure of the OLED and its energy diagram was schematically illustrated in figure 4.4. The total thickness of TPBi as an ETL was designed to 150 nm. This structure is not optically good for having high efficiency OLEDs, which was supported by optical simulation of EQE shown in figure 4.5. However, the effect of the vertically aligned dipole could be enlarged in this structure. The Rb_2CO_3 was used as an n-dopant to compensate thick ETL.

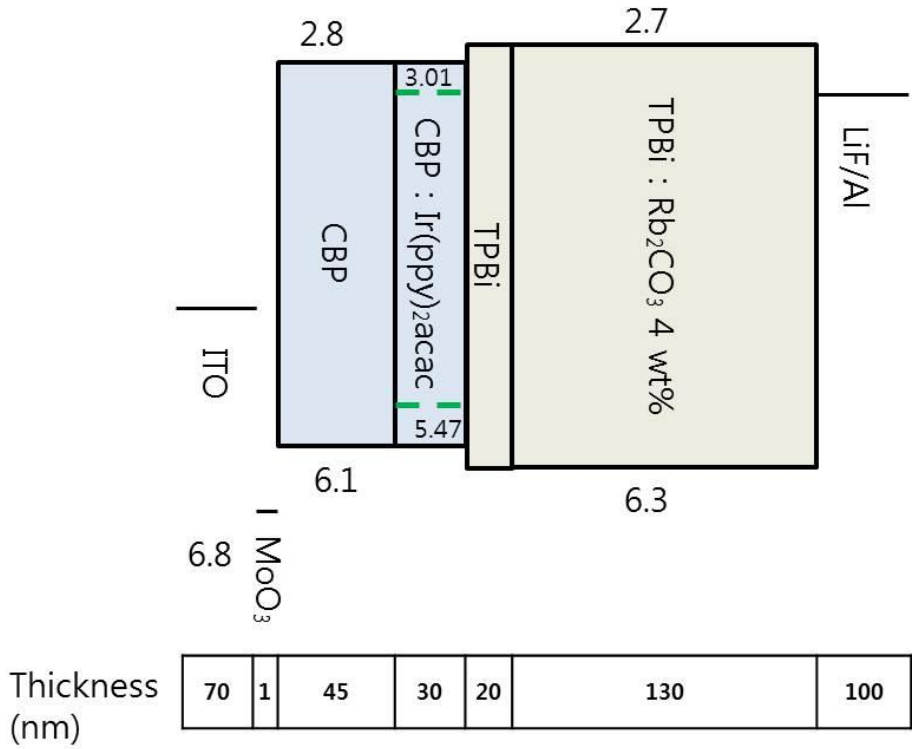

Figure 4.4 Device structure and schematic energy diagram of the OLEDs.

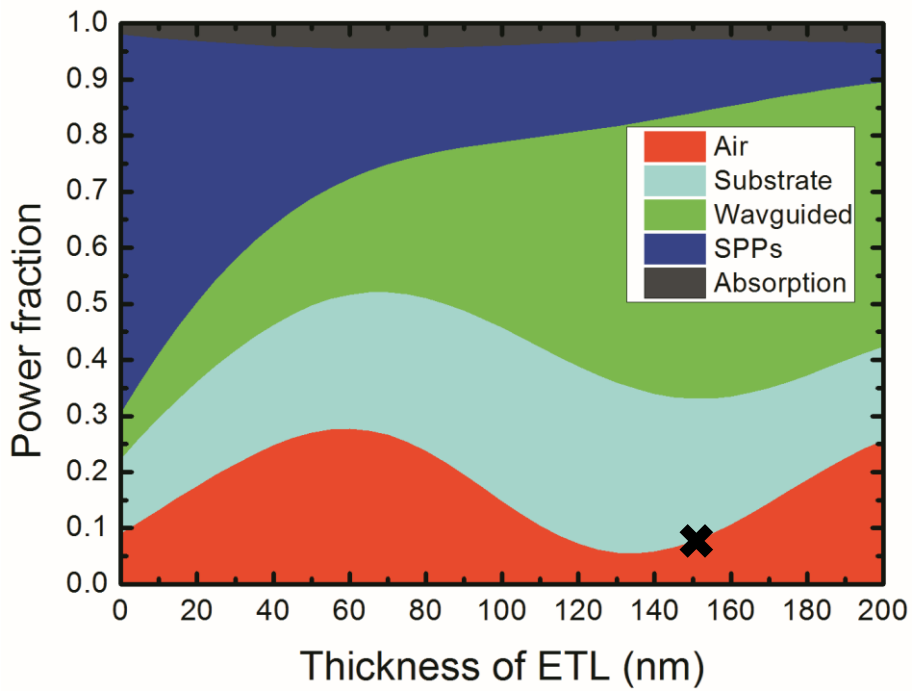

Figure 4.5 The mode analysis of OLEDs as a function of the ETL thickness. The red area shows the EQE of OLEDs. The x mark indicates the thickness of actual devices.

4.3.2 Device characteristics

Figure 4.6 shows the current-voltage-luminescence (J-V-L) characteristics of the OLEDs in log and linear scale. Current density of the OLED 1 was 1.6 times larger than that of the OLED 2 at the same voltage after turned on. However, the OLED 2 showed 1.4 times larger luminescence than the OLED 1. The J-V curves said that when the concentration of emitter was high, emitter molecules could affect to current density as trap sites in this device structure**.** However, the luminescence was not different as much as concentration difference. It suggested that the $Ir(ppy)_2acac$ was excited by energy transfer from CBP rather than by direct trap assist recombination at low doping concentration.

Figure 4.7a and 4.7b shows EL spectra at normal direction with increasing driving voltages. The emission of CBP was observed in the OLED 1 but not in the OLED 2. It also supported the energy transfer in the low concentration device. The spectrum shift with the increasing driving voltage was observed in both OLEDs. It can be interpreted that the recombination zone shifted. The comparison of spectra of two OLEDs at same voltage is illustrated in figure 4.7c. The difference of spectral peak was same with a red-shift by doping concentration observed in PL spectra. Therefore, the OLED 1 was considered to have a similar tendency of the recombination zone shift.

Figure 4.8a shows angle-dependent EL spectra of the OLED 2 at constant current density 7.5 mA/cm^2 (~ 8.4V). The angular intensity distribution was 0.72 times smaller than the Lambertian distribution. The OLEDs 1 was considered to have similar distribution with the OLED 2. After the angular calibration, the maximum external quantum efficiencies of the OLED 1 and the OLED 2 were obtained 1.6% and 3.6%.

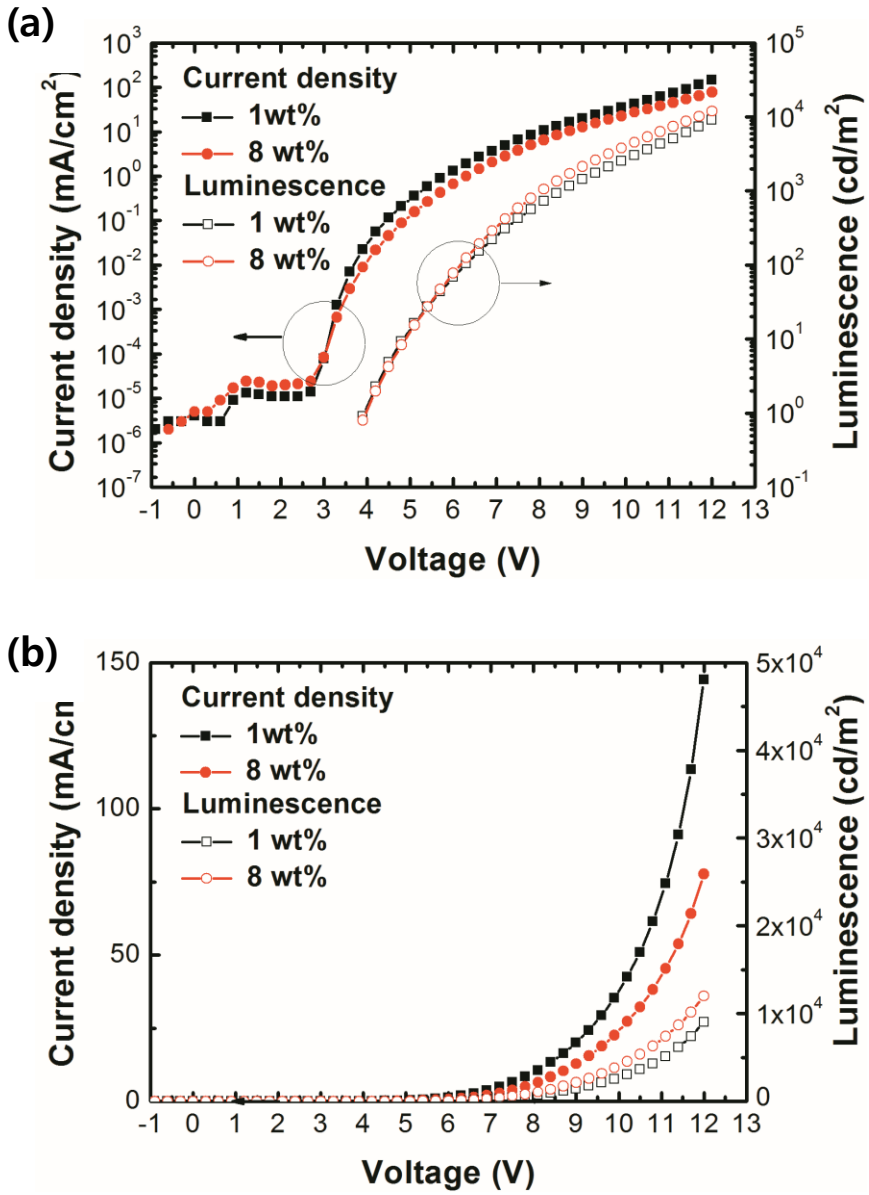

Figure 4.6 The J-V-L characteristics depending on applied voltage in (a) log and (b) linear scale.

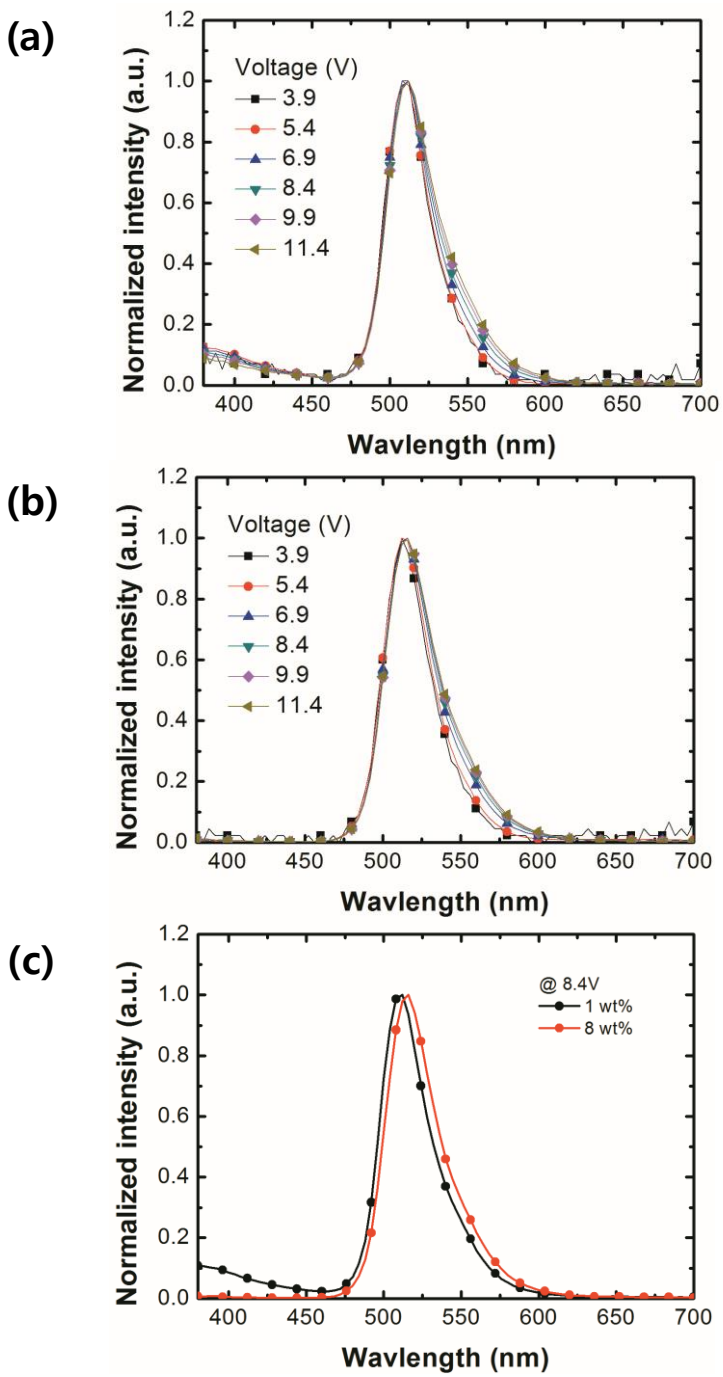

Figure 4.7 EL spectra vs. voltage of the (a) OLED 1 and (b) OLED 2. (c) EL spectra of two OLEDs at same voltage 8.4 V.

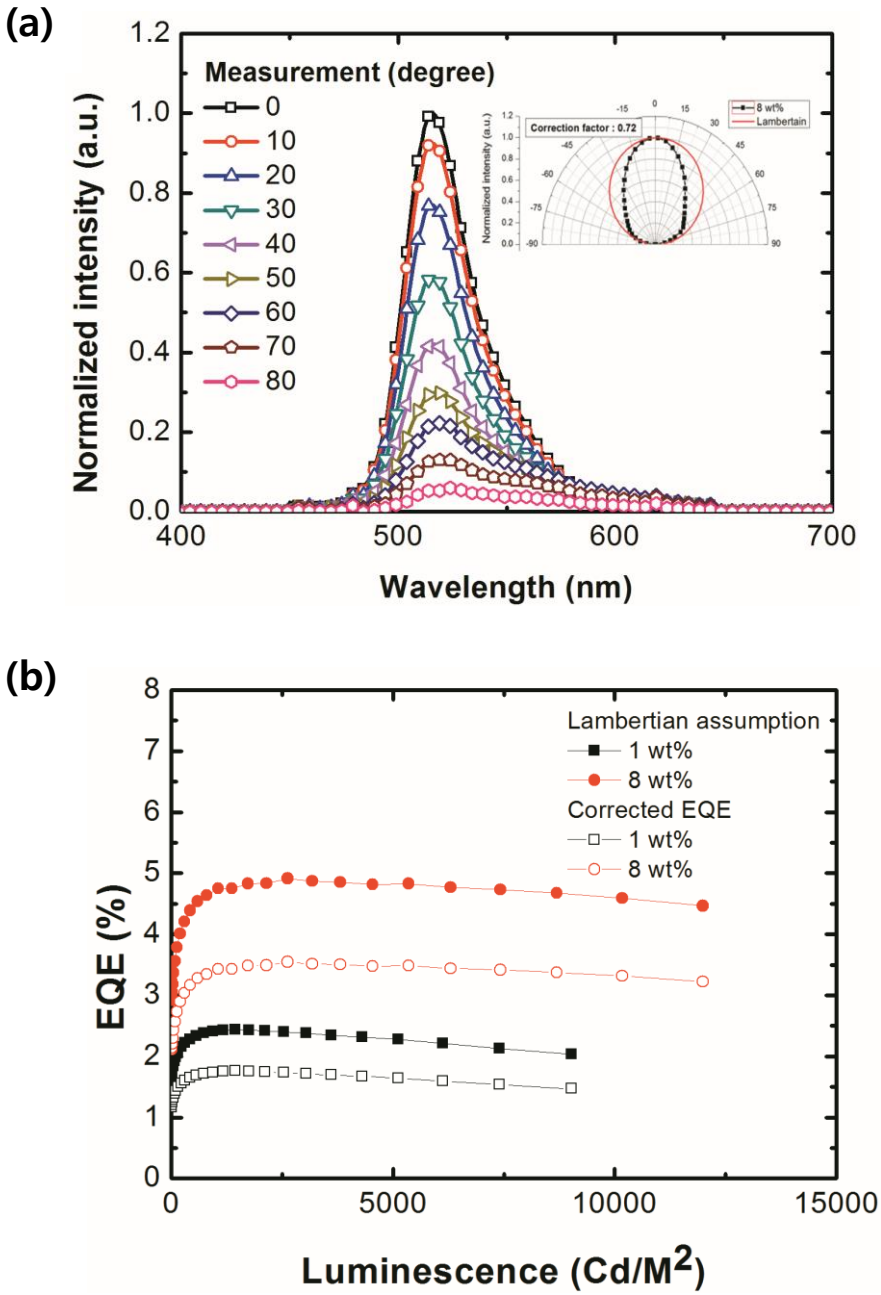

Figure 4.8 (a) Angular EL spectra of the OLED 2 at constant current density 7.5 mA/cm^2 (~ 8.4V) (b) EQE vs. luminescence curves after the angular calibration.

4.3.3 Determination of the recombination zone

The recombination zone should be determined for analysis of the dipole orientation. By comparison of experimental results and simulation, the mean recombination zone which was assumed to be as a sheet in the EML could be determined. The emission spectra at normal direction and the angle-dependent EL spectra of the OLED 2 were analyzed with the optical simulation. According to the optical simulation, the mean recombination zone shifted toward the EML/HTL interface from center of the EML as driving voltage increased. Figure 4.9a shows fittings of the measurements and simulation of emission spectra at normal direction. This recombination zone shift was also supported by angle-dependent EL spectra. The spectra were measured at constant current density 7.5 mA/cm^2 and driving voltage about 8.4V. Therefore, the recombination zone could be assumed to be a sheet which apart 25 nm from the ETL/EML interface through the spectrum-voltage results. The optical simulation of angle-dependent EL spectra for that recombination zone matched well with the measurements as shown in figure 4.9b.

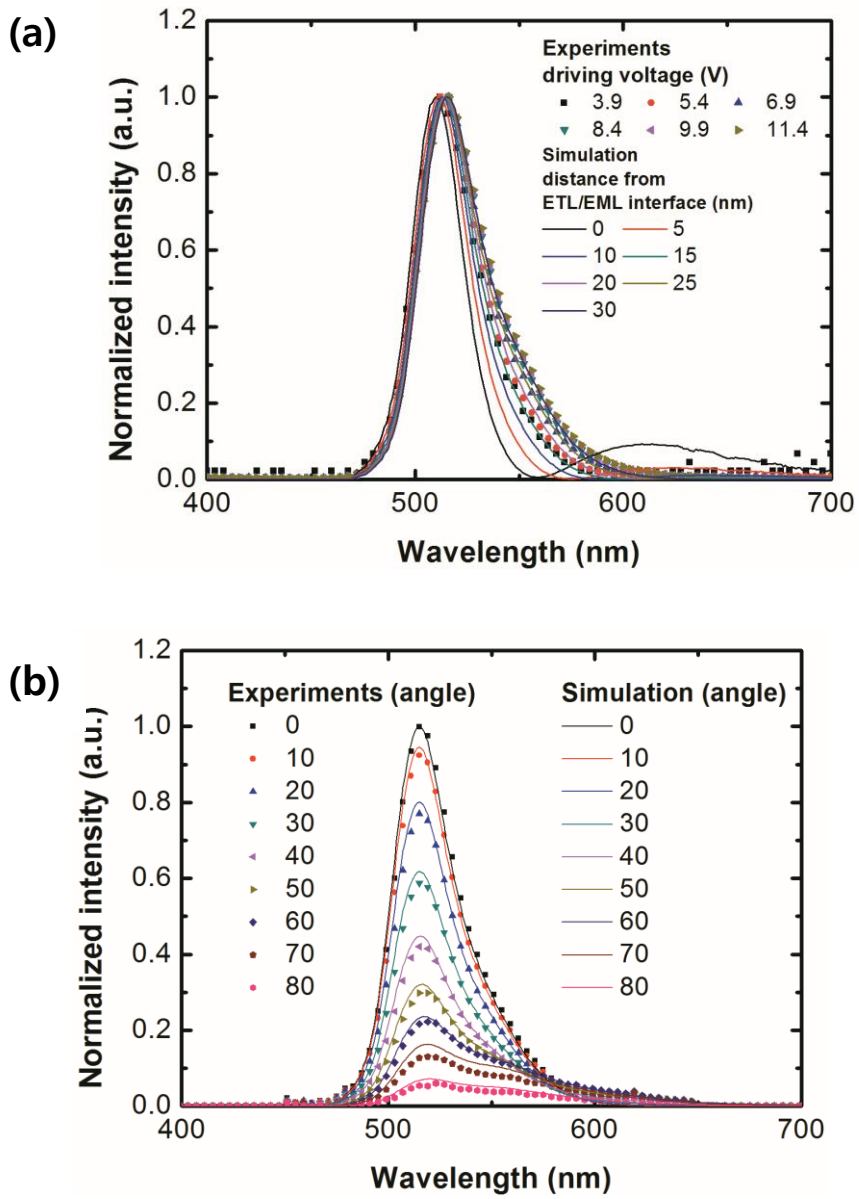

Figure 4.9 Comparisons of the measurements and simulation of the OLED 2. The simulation shows (a) emission spectra at normal direction with variation of recombination zone from the ETL/EML interface, (b) angle-dependent EL spectra at 25 nm recombination zone from the ETL/EML interface.

4.3.3 Dipole orientation of $Ir(ppy)_2acac$ in OLEDs

To find out the orientation of $I(rppy)_2acac$ in OLEDs, the angle-dependent EL pattern at 520 nm wavelength was measured in the same set-up of angle-dependent PL measurement with a little modification. A current source with conduction wires was used for electrical excitation instead of a laser as shown in figure 4.10. Constant electric current density 7.5 mA/cm^2 (~8.4V) to both OLEDs was given during measurement. Optical simulation for angular emission pattern of these OLEDs was practiced with the recombination zone which is 25 nm from the ETL/EML interface. Measurements and their fittings by simulation are illustrated together in figure 4.11. Interestingly, angular emission patterns with electrical driving were differed with dye concentration as shown in PL experiments. With optical simulation, the value of α was determined to 0.72for the OLED 1 and 0.75 for the OLED 2. It agreed well with the orientation determined in PL experiment.

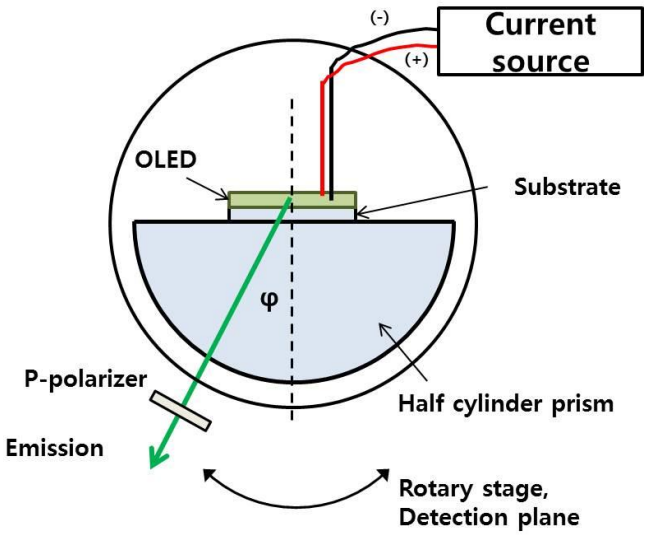

Figure 4.10 A schematic illustration of a set-up for angle-dependent EL measurement. Keithley 2400 was used as an electric current source.

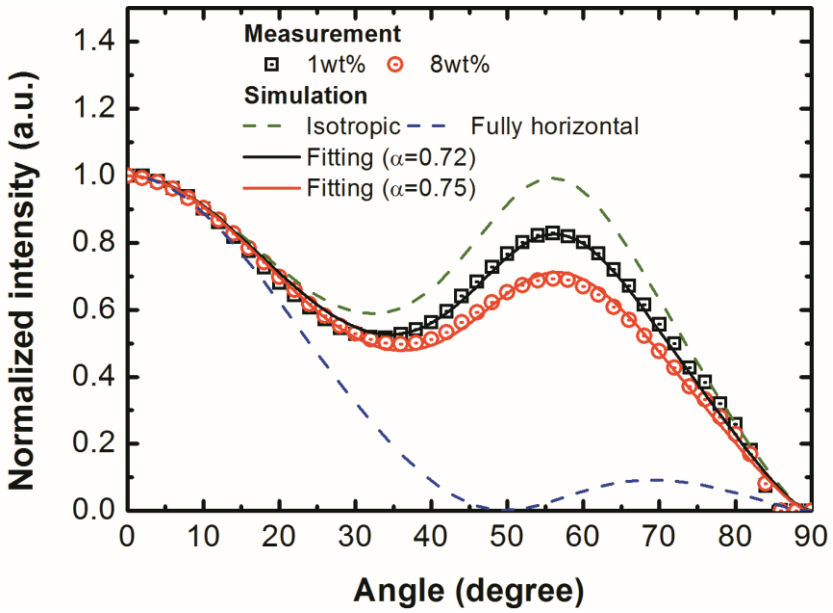

Figure 4.11 Results of angle-dependent EL measurement of the OLED 1 and OLED 2. The emission pattern of the OLED 1 fitted when α = 0.72 and the OLED 2 fitted when α = 0.75.

4.4 Dipole orientation of $Ir(ppy)_2acac$ in the energy-transferring condition

4.4.1 Absorption characteristics and direct dopant excitation condition

Figure 4.12 shows absorption characteristics of CBP and $Ir(ppy)_2acac$. The absorbance of CBP was measured as a 50 nm thick film. It absorbed light shorter than 370 nm wavelength without consideration of the absorbance tail. The extinction coefficient (ε) of $Ir(ppy)_2acac$ was measured as 0.01M dilute solution in methylene chloride. It shows that the $Ir(ppy)_2acac$ can absorb light shorter than 510 nm wavelength. A direct dopant excitation condition could be made by using a 405 nm laser for excitation. Dipole orientation of $Ir(ppy)_2acac$ was analyzed in the direct dopant excitation condition compared to the energy-transferring condition.

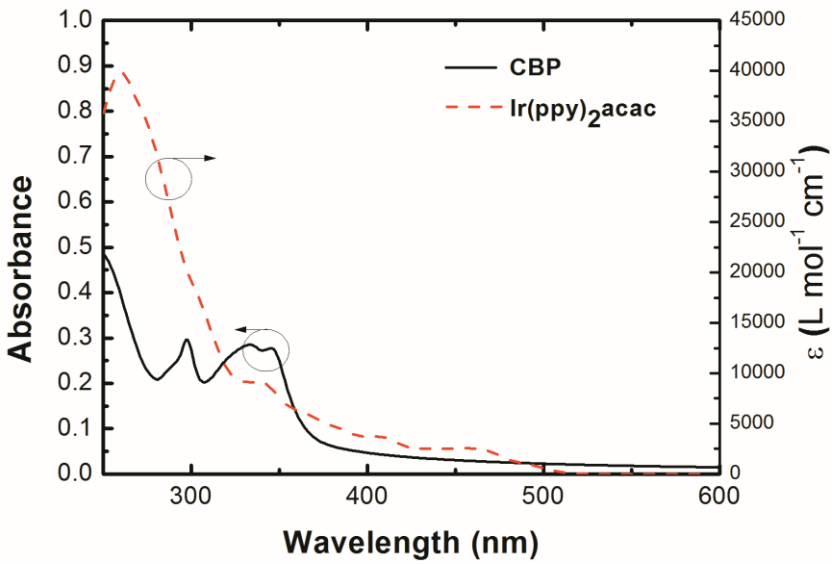

Figure 4.12 Absorption characteristics of CBP and $Ir(ppy)_2acac$.

4.4.2 PL spectra in the direct dopant excitation condition

PL spectra of the CBP:Ir(ppy)$_2$acac films were measured with the 405 nm excitation. As shown in figure 4.13, there was no emission of CBP, which proved that the direct dopant excitation condition was made. The PL intensity of Ir(ppy)$_2$acac kept increasing from concentration of 0.1 wt% to 16 wt% because the amount of emitting molecules increased. Shapes of Ir(ppy)$_2$acac emission at each concentration were same independent of excitation wavelength as shown in inset of figure 4.3, which meant that there was no change of energy state between two different excitation methods.

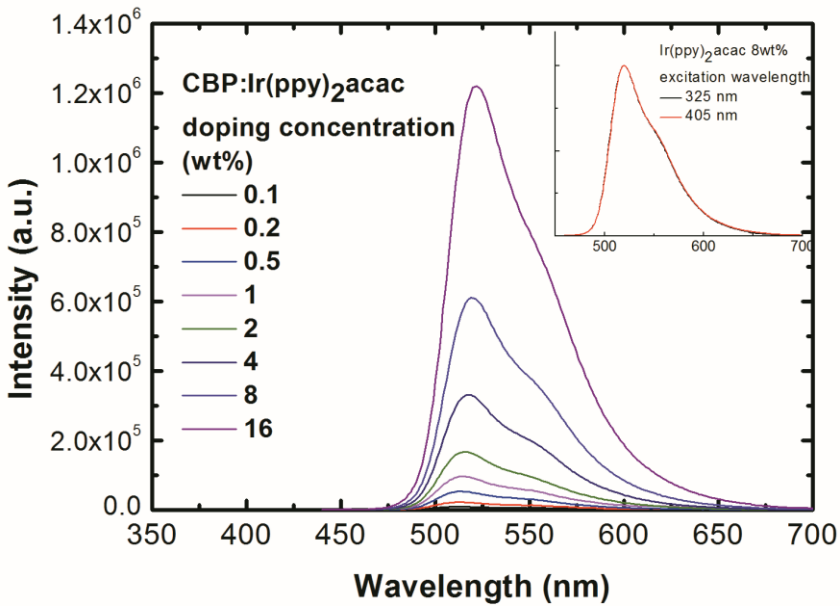

Figure 4.13 PL spectra of CBP:Ir(ppy)$_2$acac films depending on doping concentration with the 405 nm excitation.

4.4.3 Angle-dependent PL pattern in the direct dopant excitation condition

Angle-dependent PL patterns in the direct dopant excitation condition didn't change with doping concentration unlike in the energy-transferring condition as shown in figure 4.14. These results supported that the change of PL patterns in the energy-transferring did not come from film uniformity such as film thickness and refractive index but from the excitation method. It meant that the dipole orientation changed with the doping concentration only in the energy-transferring condition. The PL patterns were fitted well when the value of α is 0.75, which were identical to that in the energy-transferring condition at high concentration.

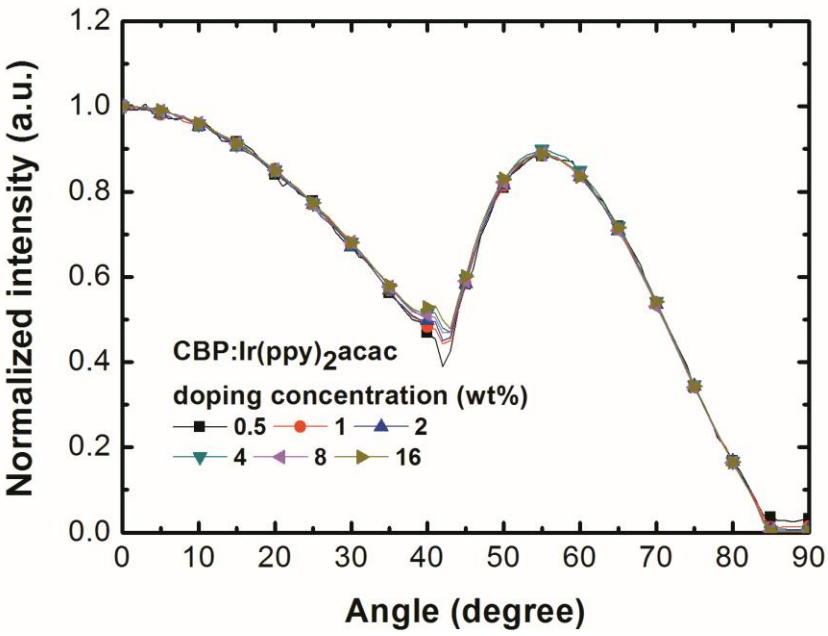

Figure 4.14 Angle-dependent PL pattern of CBP:Ir(ppy)$_2$acac films. The patterns were same independent of the doping concentration.

4.4.4 Doping concentration dependence dipole orientation

Figure 4.15 shows comprehensive doping concentration dependence of dipole orientation of $Ir(ppy)_2acac$ in the CBP matrix. The tendencies were different with the excitation condition. Frist, in the energy-transferring condition, the proportion of the horizontal dipole of $Ir(ppy)_2acac$ was 75% at the high enough doping concentration but it kept decreasing as the doping concentration decreased from 8 wt%. This phenomenon was also shown in OLEDs with the electric driving. The 1 wt% and 8 wt% $Ir(ppy)_2acac$ doped OLEDs was had 70% and 75% horizontal dipole each which were identical to that investigated in films. Both films and OLEDs emitted light by energy transfer from CBP host. Second, in the direct dopant excitation condition, the dipole orientation did not change with the doping concentration. The cause is not clear yet, but one suggestion is that the dipole orientation of energy acceptor could be modified by direction-dependent enhancement of energy donor molecules when the donor emission was remained. When the dipole moment of donor molecules were modified by electric fields themselves, they will give energy to acceptor molecules not equally. Therefore, the intrinsic dipole orientation in the direct dopant condition and effective dipole orientation in the energy transferring condition can be different.

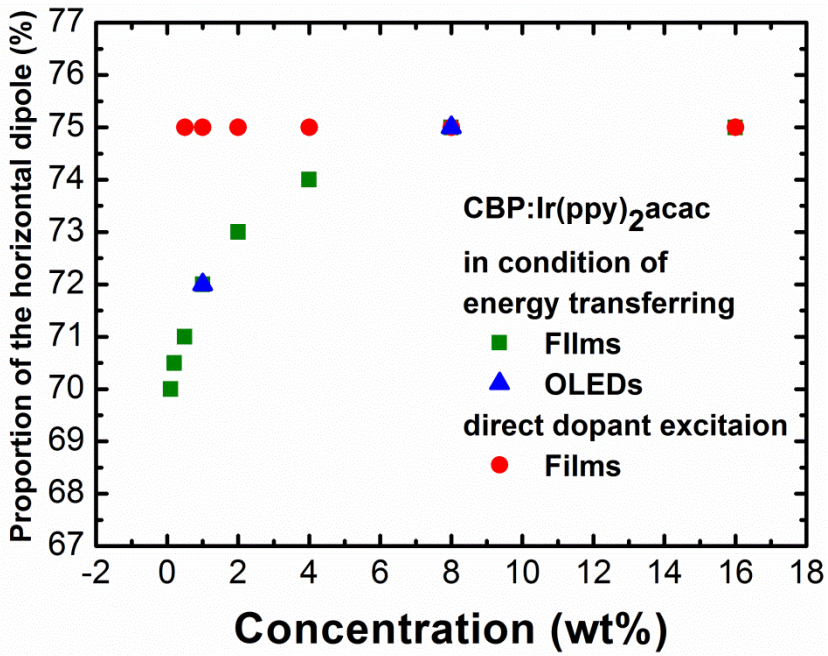

Figure 4.15 Doping concentration dependence of dipole orientation of $Ir(ppy)_2acac$ in the CBP matrix.

Chapter 5. Summary and conclusion

The dipole orientation of phosphorescent dyes doped in CBP host was studied. First, I improved the angle-dependent PL method to obtain symmetrical and reproducible results. Next, dipole orientation of 6 different phosphorescent dyes of FCNIr, FIrpic, Ir(ppy)3, $Ir(ppy)_2acac$, $Ir(piq)_3$, and $Ir(MDQ)_2acac$ was determined by this modified method. Each dyes had its own dipole orientation although their structures are globular. The dipole orientation was different with types of main ligand, ancillary ligand and substituents. Moreover, other factors that affect to the dipole orientation were investigated. As a result, the doping concentration and the excitation condition affect to the orientation. The proportion of the horizontal dipole reduced as the doping concentration decreased in the energy-transferring condition. This phenomenon was shown both in PL experiments of films and EL experiments of OLEDs. However, that was not observed in the direct dopant excitation condition. Therefore, I suggested concepts of the intrinsic dipole orientation and the effective dipole orientation in the energy-transferring condition. In conclusion, the dipole orientation of phosphorescent Ir complexes was analyzed that it was influenced by molecular structure, doping concentration, and excitation condition.

Reference

[1] S.-Y. Kim, W.-I. Jeong, C. Mayr, Y.-S. Park, K.-H. Kim, J.-H. Lee, *et al.*, "Organic Light-Emitting Diodes with 30% External Quantum Efficiency Based on a Horizontally Oriented Emitter," *Advanced Functional Materials*, vol. 23, pp. 3896-3900, 2013.

[2] W. Brütting, J. Frischeisen, T. D. Schmidt, B. J. Scholz, and C. Mayr, "Device efficiency of organic light-emitting diodes: Progress by improved light outcoupling," *physica status solidi (a)*, vol. 210, pp. 44-65, 2013.

[3] M. Furno, R. Meerheim, S. Hofmann, B. Lüssem, and K. Leo, "Efficiency and rate of spontaneous emission in organic electroluminescent devices," *Physical Review B*, vol. 85, 2012.

[4] E. M. Purcell, *Phys. Rev.*, vol. 69, pp. 681–681, 1946

[5] R.R. Chance, A. Prock, R. Silbey, *Adv. Chem. Phys.*, vol. 37, p. 1, 1978

[6] W. L. Barnes, "Fluorescence near interfaces: The role of photonic mode density," *Journal of Modern Optics*, vol. 45, pp. 661-699, 1998.

[7] J. A. E. Wasey and W. L. Barnes, "Efficiency of spontaneous emission from planar microcavities," *Journal of Modern Optics*, vol. 47, pp. 725-741, 2000.

[8] K. Neyts, "Microcavity effects and the outcoupling of light in displays and lighting applications based on thin emitting films," *Applied Surface Science,* vol. 244, pp. 517-523, 2005.

[9] H. Kuhn, "Classical Aspects of Energy Transfer in Molecular Systems," *The Journal of Chemical Physics,* vol. 53, p. 101, 1970.

[10] C. W. Tang and S. A. VanSlyke, "Organic electroluminescent diodes," *Applied Physics Letters,* vol. 51, p. 913, 1987.

[11] D. I. S. Charalambos C. Katsidis, "General transfer-matrix method for optical multilayer systems with coherent, partially coherent, and incoherent interference," *Appl.Opt,* vol. 41, p. 4978, 2002.

[12] Y.-S. Park, S. Lee, K.-H. Kim, S.-Y. Kim, J.-H. Lee, and J.-J. Kim, "Exciplex-Forming Co-host for Organic Light-Emitting Diodes with Ultimate Efficiency," *Advanced Functional Materials,* vol. 23, pp. 4914-4920, 2013.

[13] S. Lee, K.-H. Kim, D. Limbach, Y.-S. Park, and J.-J. Kim, "Low Roll-Off and High Efficiency Orange Organic Light Emitting Diodes with Controlled Co-Doping of Green and Red Phosphorescent Dopants in an Exciplex Forming Co-Host," *Advanced Functional Materials,* vol. 23, pp. 4105-4110, 2013.

[14] J. B. Kim, J. H. Lee, C. K. Moon, S. Y. Kim, and J. J. Kim, "Highly enhanced light extraction from surface plasmonic loss minimized organic light-emitting diodes," *Adv Mater,* vol. 25, pp. 3571-7, Jul 12 2013.

[15] J. H. Lee, S. Lee, J. B. Kim, J. Jang, and J. J. Kim, "A high performance transparent inverted organic light emitting diode with 1,4,5,8,9,11-hexaazatriphenylenehexacarbonitrile as an organic buffer layer," *Journal of Materials Chemistry,* vol. 22, pp. 15262-15266, 2012.

[16] L. Penninck, F. Steinbacher, R. Krause, and K. Neyts, "Determining emissive dipole orientation in organic light emitting devices by decay time measurement," *Organic Electronics,* vol. 13, pp. 3079-3084, 2012.

[17] P. Liehm, C. Murawski, M. Furno, B. r. Lüssem, K. Leo, and M. C. Gather, "Comparing the emissive dipole orientation of two similar phosphorescent green emitter molecules in highly efficient organic light-emitting diodes," *Applied Physics Letters,* vol. 101, p. 253304, 2012.

[18] T. D. Schmidt, D. S. Setz, M. Flämmich, J. r. Frischeisen, D. Michaelis, B. C. Krummacher, *et al.*, "Evidence for non-isotropic emitter orientation in a red phosphorescent organic light-emitting diode and its implications for determining the emitter's radiative quantum efficiency," *Applied Physics Letters,* vol. 99, p. 163302, 2011.

[19] J. Frischeisen, D. Yokoyama, A. Endo, C. Adachi, and W. Brütting, "Increased light outcoupling efficiency in dye-doped small molecule organic light-emitting diodes with horizontally oriented emitters,"

ORGANIC ELECTRONICS, vol. 12, pp. 809-817, 2011.

[20] J. r. Frischeisen, D. Yokoyama, C. Adachi, and W. Brütting, "Determination of molecular dipole orientation in doped fluorescent organic thin films by photoluminescence measurements," *Applied Physics Letters*, vol. 96, p. 073302, 2010.

초 록

쌍극자의 방향성은 유기발광다이오드(OLEDs)의 효율에 영향을 미치는 중요한 요소이다. 고분자 또는 선형, 또는 원판형 구조를 가진 저분자들은 편향된 방향성을 가지고 알려져 있었다. 반면에 구형의 구조를 갖는 인광염료분자, 특히 이리듐 복합체의 경우 편향된 방향성을 가지지 않을 것이라고 생각되어왔다. 하지만 최근에 몇몇 임광염료들도 진공 열증착으로 박막이 형성되었을 때 기판에 평행하도록 방향성을 가지고 있다는 보고들이 있어왔다. 그러나 이러한 이리듐 복합체의 쌍극자 모멘트 방향에 영향을 주는 요소들이 아직 연구되지 않았다. 본 논문에서는 이리듐 복합체의 주 리간드와 보조리간드의 종류에 따라 어떠한 방향성을 가지는지 보고한다. 더 나아가 도핑 농도와 여기 조건이 방향성에 영향을 미치는 요소임을 연구하였다.

주요어: 유기발광다이오드, 임광염료, 쌍극자 방향성, 유효 방향성, 각도의존성 광루미네센스 측정, 광학시뮬레이션, 에너지 전달

학번: 2012-20598

감사의 글

어느덧 2년이 흘러 저에게도 석사학위를 받는 날이 왔습니다. 아직 학생생활이 더 많이 남아있지만 이렇게 중간에 제 연구를 공식적으로 총정리하고 생각할 수 있는 기회를 가져서 좋았습니다. 많은 분들의 도움이 있었기에 이 논문이 나올 수 있었다고 생각합니다.

먼저 저에게 바른 연구인의 자세를 알려주시고 아낌없는 조언을 해 주신 김장주 교수님께 감사드립니다. 또한 바쁜 와중에도 학위심사를 지도해 주신 윤재륜 교수님, 서용석 교수님께 감사의 말씀을 드립니다.

또한 동고동락하며 함께해준 OPL 식구들 모두에게 감사합니다. 큰형으로서 지도해 주신 성훈형, 후배들의 연구에 조언을 많이 해주시는 정환형, 인생의 지혜를 알려주시는 태민형, 항상 도움 받는다고 하지만 제가 더 많이 도움 받는 정범형, 앞으로 동생들을 잘 이끌어갈 현섭형, 가장 성실하신 대호형, 어떤 말을 해도 잘 받아주시고 아는 것도 많은 승준형, 같이 있으면 즐거운 진원형, 이제 실험실의 중심이 될 경훈형, 창헌형, 권현이 모두 도와주셔서 감사합니다. 같이 고생한 저의 동기들 민수, 범수형 우리 다 같이 잘 되리라 믿습니다. 재민이, 현이 좋은 연구 잘 마무리 되길

바라며 제가 정신 없을 때 많이 도와주신 봄이누나 현구형 감사합니다. 또한 새로 합류한 황범이, 민형이도 열심히 해서 좋은 결과를 내길 바랍니다. 실험실 초기 저의 연구방향설정과 지식을 쌓는 데에 가장 큰 도움을 주신 세용형과 학생들을 연구에 전념할 수 있도록 도와주신 지희누나께 특히 더 감사드립니다.

무엇보다도 20년 넘도록 저의 뒷바라지를 해 주신 우리 가족 아버지, 어머니, 누나 표현은 많이 못했지만 다시 한번 이렇게라도 고맙고 사랑한다고 말하고 싶습니다. 앞으로 더욱 정진해 나가겠습니다.

2013년 1월 27일

문창기